Energy and intensity distributions of multiple Compton scattering of 0.279-, 0.662-, and 1.12-MeV γ rays

Manpreet Singh, Gurvinderjit Singh, Bhajan Singh, and B. S. Sandhu*
Physics Department, Punjabi University, Patiala-147002, India
(Received 27 February 2006; published 13 October 2006)

Multiple Compton scattering results in an incorrect evaluation of Compton profile, which usually examines the case when the photon has undergone only one Compton collision in the sample. The probability of a photon being scattered several times may be significant for a target of finite dimensions both in depth and lateral dimensions. The present measurements are carried out to study the energy and intensity distributions of 0.279, 0.662, and 1.12 MeV γ rays multiply scattered from the copper target of various thicknesses at a scattering angle of 60°. The scattered photons are detected by a NaI(Tl) scintillation detector whose detector response unfolding, converting the pulse-height distribution to a photon energy spectrum, is obtained with the help of an inverse response matrix. We observe that with an increase in target thickness, the number of multiply scattered photons saturates at a particular value of the target thickness (saturation depth). The multiply scattered fraction starts saturating above a particular energy window around the centroid of inelastic scattered peak. The signal-to-noise ratio is found to be decreasing with an increase in target thickness. Monte Carlo calculations based upon the package developed by Bauer and Pattison [Comptom Scattering Experiments at the HMI (1981), **HMI-B 364**, pp. 1–106] support the present experimental results.

DOI: 10.1103/PhysRevA.74.042714 PACS number(s): 32.80.Cy, 13.60.Fz, 78.70.−g

I. INTRODUCTION

A correct evaluation of a Compton profile, used as a means for determination of the electron momentum distribution [1], requires that the photon scattered by the sample should have undergone only one Compton collision. In actual practice, the interactions of photons with the target result in a significant fraction of multiply scattered photons in addition to singly scattered ones. The energy spectrum of such photons is broad and never completely separate from the singly scattered distribution in actual measurements. This leads to the smearing of information associated with the intensity change of scattered photons, since the singly scattered distribution comes from the overlap volume defined by the intersection of the incoming beam and the detector collimation, while the multiply scattered photons practically may come from the whole sample. Photons continue to soften in energy as the number of scatterings increases in the sample. Thus, an accurate measurement of intensity and energy distributions of multiply scattered photons is required at different scattering angles in various materials as a function of target thickness and incident photon energy to correct the data for multiple scattering contaminations.

A complete survey of analytical and Monte Carlo simulation approaches to study the multiple scattering has been given in our previous measurements [2], to which one may refer for literature on this study. The experimental measurements of Williams and Halonen [3] and of Halonen *et al.* [4] provide intensity and spectral distributions of the double scattering in aluminum with different sample thicknesses for 59.54 keV incident photons scattered through 150°. Halonen and Williams [5] calculated the angular distribution of the double scattering for aluminum and nickel using the relativistic Klein-Nishina cross section and applied these results to experimental Compton profiles of aluminum and nickel measured at 60 and 159 keV in order to correct for multiple scattering.

At 662 keV, Paramesh *et al.* [6] measured the saturation depth of multiply scattered γ rays by subtracting the analytically evaluated contribution of singly scattered γ rays at 120° for aluminum, iron, copper, and lead. Pitkanen *et al.*, [7] have measured the spectrum of 662 keV γ rays multiply scattered from a nickel sample at a scattering angle of 104° and simulated the experimental data by the Monte Carlo method to correct the single scattered line shapes. Later, these authors [8] carried out calculations using extensive Monte Carlo simulations of the multiple scattering contamination in Compton scattering studies for the exact determination of the electron momentum distribution in an atom at various incident energies ranging from 60 to 662 keV in a number of elements (Z=6–38). Barnea *et al.*, [9] measured the distribution of multiply scattered photons at 662 keV for samples of aluminum, brass, and tin at 90° and 120°, and compared the experimental results to the Monte Carlo simulations (ACCEPT code in ETRAN model) developed according to the geometrical setup of their experiment. Shengli *et al.* [10] have performed multiple scattering experiments to detect an iron object embedded in the large concrete wall at 662 keV using a NaI(Tl) scintillation detector. By simulating their experiment with the Monte Carlo simulation in the EGS4 package, they concluded that the presence of multiple Compton scattering impairs the contrast between the background and the object. Our previous measurements [2] are confined to the effect of the detector collimator and the sample thickness on 0.662 MeV multiply Compton scattered photons from cylindrical samples of aluminum, and confirmed that in order to increase the signal-to-noise ratio, multiple scattering background should be minimized and can be

*Corresponding author. FAX: 91 175 2286412. Email address: balvir@pbi.ac.in and balvir99@indiatimes.com

 ©2006 The American Physical Society

achieved by using a narrow detector collimation. The multiply scattered fraction (MSF) increases and saturates with an increase in the energy window around the Compton scattered peak.

In spite of extensive investigations of multiple scattering by means of Monte Carlo methods or by analytical treatment of photon transport, the experimental data of multiple scattering of γ rays available so far are limited to few incident photon energies. There are no experimental data available on multiple scattering of 0.279 and 1.12 MeV incident photons. In view to get useful information on the multiple scattering of 0.279, 0.662, and 1.12 MeV γ rays, the present experiments are performed to determine the energy and intensity distributions of multiply scattered photons from copper targets of various thicknesses at 60° scattering angle. The scintillation detector response unfolding, converting the pulse-height distribution to a photon energy spectrum is obtained with the help of an inverse response matrix. The choice of a 60° scattering angle results in a singly scattered Compton peak distribution lying completely in one of the selected energy bin meshes chosen for scintillation detector response unfolding. The saturation thickness, MSF and signal-to-noise ratio are also reported.

II. METHOD OF MEASUREMENTS

There exist three different approaches [11] for the evaluation of multiple scattering of γ rays in Compton profiles measurements. The first method involves changing the geometry of the scattering body in such a way that the fraction of events involving more than one scattering is reduced. Here the most obvious approach is to use a series of samples of different thicknesses and extrapolate the results to zero thickness. However this simple extrapolation procedure is unsuitable because the functional dependence of the multiple scattering intensity on sample thickness is quite complex and is nonlinear even for relatively thin samples. In addition, equally important is the often-ignored assumption that the shape of the multiple scattered profiles is independent of sample thickness. In the second approach, the amount of multiple scattering can be determined directly by using a displaced beam technique to eliminate the single scattering. However, the geometry of the scattering depends on the displacement so that an extrapolation to zero displacement must still be made if this method is used to correct for multiple scattering. Finally, in the third approach one can calculate the intensity and spectral distributions of multiple scattering events for a given experimental arrangement using experimentally determined parameters in the calculations and use the results to correct the measured Compton profile. The intensity, spectral, and energy distribution of multiple scattering depends upon the geometry and on the properties of the beam. The present measurements employ the third method listed above and the experiment is designed to detect the flux of emergent photons from the scatterer at a scattering angle of 60°. In order to determine the contribution of multiply scattered photons only, the spectrum of singly scattered photons is reconstructed analytically as outlined below.

Consider the Compton scattering arrangement shown in Fig. 1, which also confirms that with increase in target thickness, the angle θ remains the same, but θ_1 continues to change. The two specified angles are related by the following equation:

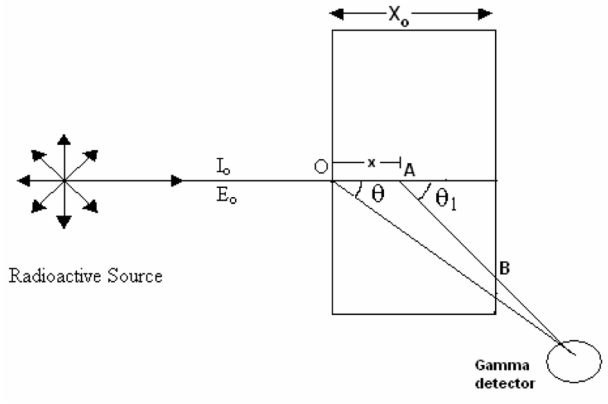

FIG. 1. Compton scattering setup showing variation of angle θ_1 with increase in distance x.

$$\cot \theta_1 = -\frac{x}{R_o \sin \theta} + \cot \theta, \tag{1}$$

where R_o is the distance between the detector and the front face of the copper target, x is the distance of the scattering point from the front face of the copper target, and θ is the scattering angle for photons scattered from the front face of the target in the direction of the γ detector. As a result of the increase in the value of x, the scattering angle (θ_1) corresponding to different points in the target along the direction of propagation of primary γ beam increases. The photons scattered at several points of the target contribute to the scattered energy that continuously decreases, requiring different values of the detector efficiency and the FWHM of the γ detector corresponding to the scattered energy (E), given by

$$E = \frac{E_o}{1 + \frac{E_o}{m_o c^2}(1 - \cos \theta)}, \tag{2}$$

where E_o is the energy of the incident photons and $m_o c^2$ is the rest mass energy of electron.

The numbers of singly scattered photons originating from the target of thickness, X_o, in the direction of the detector are found by evaluating the integral

$$n(E) = \frac{C}{X_o} \int_0^{X_o} n_e e^{-\mu_i x} \left(\frac{d\sigma}{d\Omega} \right)_{\theta_1} e^{-\mu_t x_t} d\Omega \, dx, \tag{3}$$

where C is the incident photon flux at the target; n_e is the number of electrons/cm^3 of the target; x_t equals to distance AB of Fig. 1; and μ_i and μ_t are the total attenuation coefficients of the target at incident energy (E_o) and singly scattered energy (E), respectively. The factors $e^{-\mu_i x}$ and $e^{-\mu_t x_t}$ represent the attenuation of incident photons in the target prior to scattering and the attenuation of scattered photons emerging from the target, respectively. The quantities $(d\sigma/d\Omega)_{\theta_1}$ and $d\Omega$ are the Klein-Nishina cross section at an angle θ_1 and the solid angle subtended by the γ detector at

the scattering point of the target, respectively. When incident on the detector, $n(E)$ gives rise to a pulse-height distribution, whose photopeak at an energy E can be represented by a Gaussian distribution $Y(E')$ with an area given by

$$A = n(E)\varepsilon_i(E)\varepsilon_p(E), \tag{4}$$

where the quantity $\varepsilon_i(E)$ is the intrinsic (crystal) efficiency of the γ detector and $\varepsilon_p(E)$ is the peak-to-total ratio at the energy E.

Further, for the Gaussian distribution, one has

$$Y(E') = Y_o \exp\left\{-\frac{(E'-E)^2}{b}\right\}, \tag{5}$$

where $b=(\Delta E)^2/4\ln(2)$, and ΔE is the full width at half maximum (FWHM) of the detector corresponding to the energy E. The area under this Gaussian peak can be expressed as

$$A = 1.064 Y_o \Delta E \tag{6}$$

Then, the Gaussian distribution $Y(E')$ corresponding to each energy E is calculated using values of Y_o (peak height of the measured spectrum) and the FWHM (ΔE) of the NaI(Tl) detector. The $Y(E')$ is numerically integrated by Simpson's rule over the energy range corresponding to end points energies of the inelastic peak observed in energy spectra to obtain the total number of photons at the desired energy. The resulting distribution is the analytically estimated singly scattered profile as seen by the detector. This singly scattered spectrum is normalized at a full energy peak of the measured pulse-height distribution to obtain the contribution of singly scattered photons under the measured spectrum. This normalized peak intensity distribution is then divided by peak-to-total ratio of the detector corresponding to peak energy, and is subtracted from the observed scattered spectrum to obtain the events originating from multiple scattering.

III. EXPERIMENTAL SETUP

The present measurements are performed using ^{203}Hg (0.279 MeV), ^{137}Cs (0.662 MeV), and ^{65}Zn (1.12 MeV) radioactive sources of activity 25 mCi (1 Ci=37 GBq), 6 Ci and 43.5 mCi, respectively. The ^{203}Hg radioactive source is a compound of Hg_2O_3 sealed in a stainless steel cylindrical capsule (length 16 mm and diameter 11 mm) and is placed at the end of a cylindrical cavity of depth 20 mm and diameter 11 mm fabricated in a lead cube having each side 160 mm (Fig. 2). An aluminum hollow sleeve of an internal diameter 12 mm, fitted in the center of a rectangular block of lead having dimensions 80 mm×80 mm×15 mm, is placed coaxially adjacent to the cavity to obtain a narrow beam of 0.279 MeV γ photons. The distance of the copper scatterer from the source collimator is kept 152 mm so that the angular spread due to the source collimator (radius 6 mm) on the copper target is ±2.3°. The source-target assembly is aligned in such a way that the incident photon beam is confined to the target only.

The intense collimated beam of γ photons from the radioactive source is made to impinge normally on rectangular

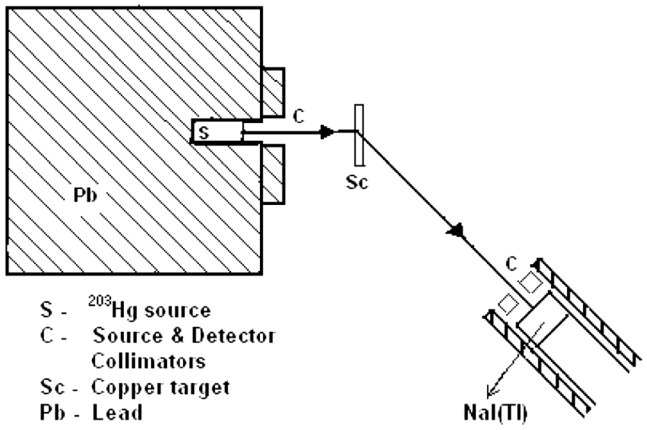

FIG. 2. Experimental arrangement for present measurements.

targets of copper of 80 mm length and 40 mm breadth of varying thickness. The radiations scattered from the target are detected by a NaI(Tl) scintillation detector having dimensions 51 mm×51 mm placed at 60° to the incident beam. The field of view of the NaI(Tl) detector is confined to the copper target only. A cylindrical collimator of lead lined with aluminum having radius 6 mm and thickness 17 mm is placed in front of the γ detector. The axes of the source collimator, γ detector, and detector collimator pass through the center of the target. The distance between the front face of the scatterer and the detector collimator (radius 6 mm) is kept 92 mm, so the angular spread about the median ray in the direction of the γ detector is ±3.7°. The scintillation detector is properly shielded by a cylindrical lead shielding having the inner side covered with 2 mm thick iron and 1 mm thick aluminum, with iron facing lead to absorb K x rays emitted by lead shielding.

The ^{137}Cs radioactive source is in the form of pellets of CsCl sealed in an aluminum can of diameter 27 mm and length 80 mm. The thickness of the walls of the aluminum can is sufficient to absorb all the β rays and 32 keV K x rays emitted due to an internal conversion process. To minimize the background and keeping in mind the biological effects of radiation, a rectangular lead container of dimensions 200 mm×160 mm×160 mm is especially prepared for the source. The cylindrical beam collimator consisting of a brass pipe and fitted with aluminum windows on both ends can be filled with a column of mercury and is used to close the beam incident on the target when desired. In the conical lead collimator another collimator of diameter 7 mm is fitted to obtain a narrow beam of γ rays. The complete source assembly (Fig. 3) is rectangular in shape, having dimensions 480 mm×320 mm×320 mm. The source container, cylindrical beam collimator, and the fine beam collimator (having 7 mm opening) are placed coaxially. When the cylindrical beam collimator is filled with a column of mercury, the background near the assembly reduces up to the natural background level and thus confirming the proper shielding of the radioactive source, which is one of the essential requirements in nuclear spectroscopy. The source and detector collimators are placed at 350 and 375 mm, respectively, from the front face of the scatterer. This results in angular spreads of ±0.6° and ±0.3° due to the source (7 mm diameter) and detector

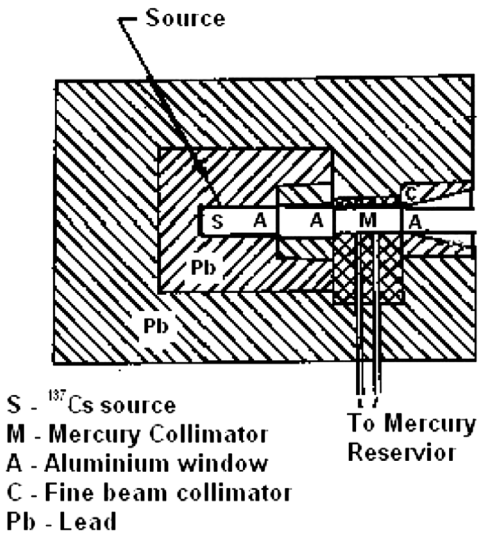

FIG. 3. Source housing of ^{137}Cs radioactive source.

collimators (4 mm diameter), respectively, on the Copper target.

The ^{65}Zn radioactive source, sealed in a stainless steel capsule (length 16 mm and diameter 11 mm), is placed in the cylindrical cavity of depth 16.5 mm and diameter 11 mm, fabricated in a lead cube having each side 320 mm (Fig. 4). A cylindrical lead cork (length 62 mm and diameter 80 mm) having an opening of 8 mm diameter is fitted permanently in the container. The collimator opening is lined with aluminum from inner sides. The distances of source and detector collimators from the front face of the scatterer are 144 and 180 mm, respectively. This results in angular spreads of ±1.6° and ±1.9° due to the source (8 mm diameter) and detector collimators (12 mm diameter), respectively, on the copper target.

The γ ray sources are placed in the respective source housings described above. The γ detector is placed at 60° to the incident beam. γ-ray spectrometer is calibrated by using

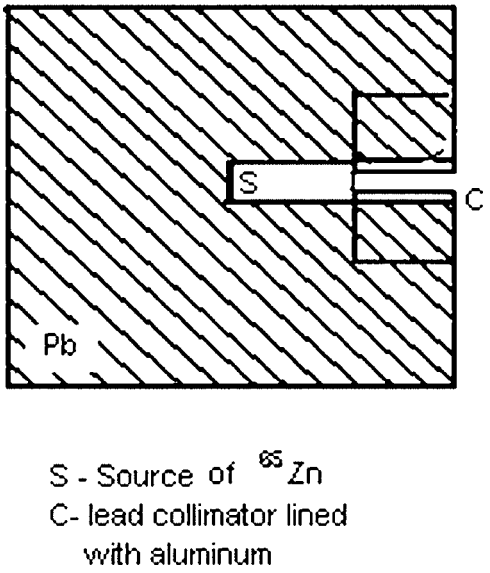

FIG. 4. Source housing of ^{65}Zn radioactive source.

standard calibration sources of different energies (^{133}Ba 0.081 and 0.356 MeV, ^{203}Hg 0.279 MeV, ^{22}Na 0.511 MeV, and ^{137}Cs 0.662 MeV). Each of the calibration sources is placed at the scatterer position and its spectrum is recorded. From the recorded spectra FWHM values corresponding to the observed full energy peaks are measured.

In the present measurements, the scattering angle of 60° has been chosen since for the three chosen incident photon energies, the singly scattered Compton peak distribution lies completely in one of the selected energy bin meshes chosen for scintillation detector response unfolding. The experimental data are accumulated on a plug-in multichannel analyzer (MCA). The measuring time for each thickness of copper target is 10 ks with the background also for the same time duration. To evaluate the true scattered spectrum for each thickness, the spectra are taken with and without scatterer in the primary beam. The stability and the linearity of the spectrometer are checked frequently and the experiment is performed in controlled temperature conditions.

IV. RESPONSE FUNCTION OF NaI(Tl) DETECTOR

The pulse-height distributions obtained when monochromatic photons are incident on a NaI(Tl) crystal consists of a peak and a continuous distribution of pulses. The conversion of such a pulse-height distribution to a photon energy spectrum is achieved with the help of a response matrix technique [12,13]. Since the width at half maximum of the photopeak varies as $E_o^{1/2}$, where E_o is the incident source energy, thus the photopeaks will be of constant width on the $E^{1/2}$ scale. Therefore a 10×10 matrix is sufficient to cover an energy range from $E^{1/2}=0.1$ to 1.0 $(\mathrm{MeV})^{1/2}$, or $E=0.01$ to 1.0 MeV. The pulse-height distributions for energies 0.279, 0.511, 0.662, and 0.834 MeV are obtained experimentally from monoenergetic sources by placing each of the sources at the copper target's position in the present experimental geometry. These are normalized in such a way that the areas under their photopeaks are made equal to intrinsic (crystal) efficiency values [14] calculated using the formula

$$\varepsilon_i(E) = 1 - e^{-\mu_{tot}(E)t}, \tag{7}$$

where $\mu_{tot}(E)$ is the attenuation coefficient for NaI(Tl) at the midpoint of source energy bin and t is the crystal thickness. These distributions are then smoothed such that peaks resulting only from the interactions after the photon entries into the crystal are included (Fig. 5), whereas those from before entry should be subtracted off. The photopeaks of these smoothed curves are omitted and their theoretical Compton edges (V_{c1}, V_{c2}, V_{c3}, and V_{c4}) are marked (Fig. 6). Then all of these four different distributions for different source energies are plotted linearly on a V/V_c scale (Fig. 7), where V_c is theoretical Compton edge for each energy. Each distribution is divided into energy bins of constant width in terms of $(E)^{1/2}$ MeV [12,13]. Labeling each bin by its top energy, the bin content distributions for the given source energies E_o, are plotted as a function of $(E')^{1/2}$. These curves are then interpolated to obtain a series of curves for each of the bins ranging from $(0.1)^{1/2}$ MeV to $(1.0)^{1/2}$ MeV in the energy range

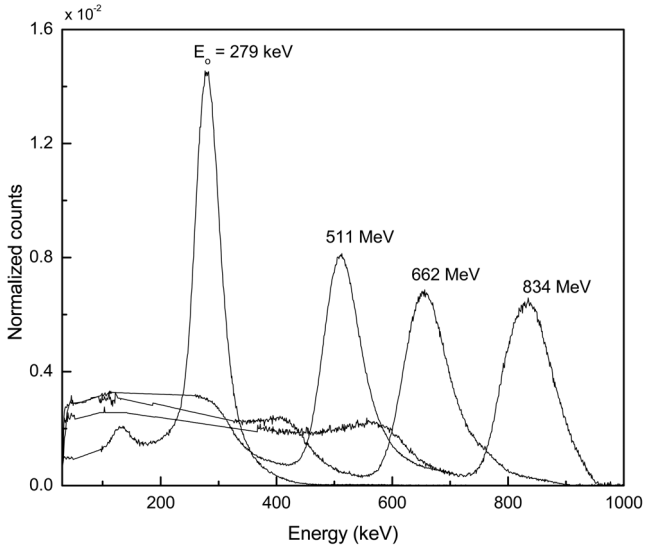

FIG. 5. Available pulse-height distributions from monoenergetic sources, areas normalized to crystal efficiency of the NaI(Tl) detector.

from 0 to 1 MeV as shown in Fig. 8. The curves having different $(E')^{1/2}$ values (Fig. 8) are then further divided into energy bins of width equal in $E^{1/2}$ MeV and the bin contents are written in the form of a triangular matrix (**R**) having elements R_{ij}, where the indices i and j refer to incident energy E and pulse height of each energy bin E'. The sum of each row is equated to $\{1-\varepsilon_p(E)\}\varepsilon_i(E)$, where $\varepsilon_i(E)$ is the intrinsic (crystal) efficiency already calculated. The photopeak efficiency $\varepsilon_i(E)\varepsilon_p(E)$ is then added to the principal diagonal of the matrix, making each row equal to $\varepsilon_i(E)$. For each ith energy, a summation over all j values equals to the crystal efficiency, the resultant matrix having elements R_{ij} given in Tables I and II is a desired response matrix, which converts spectra $N(E)$ into expected measured pulse-height distribution $S(E')$ as

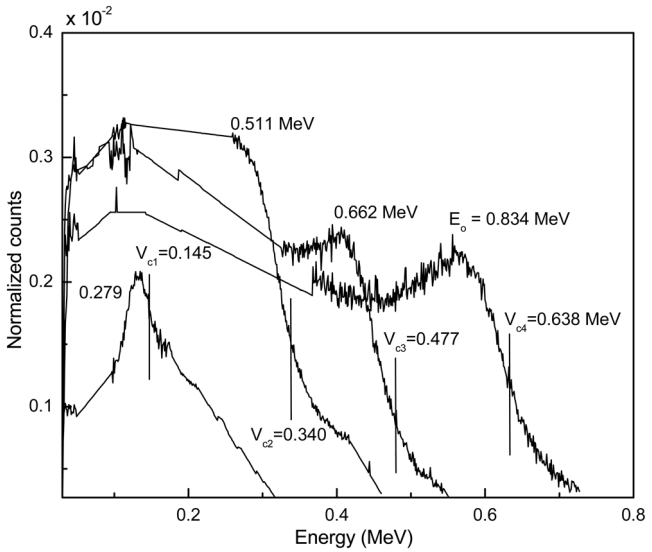

FIG. 6. Photopeaks of the curves of Fig. 5 have been subtracted off and the theoretical Compton edges, V_c, noted.

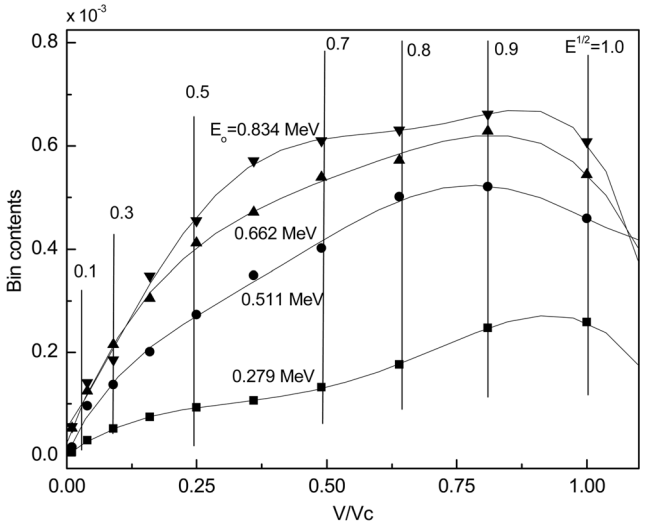

FIG. 7. Transformation to V/V_c scale, cross cuts of constant V/V_c is indicated.

$$S_j = \sum_{i=1}^{N} N_i R_{ij}, \tag{8}$$

where S_j and N_i are formed from $S(E')$ and $N(E)$ in a manner similar to R_{ij}. Therefore if we have to obtain original spectra from the measured pulse-height distribution, then the above response matrix (**R**) is to be inverted. A FORTRAN program [15] does this inversion. The response of the detector is obtained by a simple matrix multiplication of $S(E')$ and R_{ij}^{-1} as

$$N_i = \sum_{j=1}^{N} S_j R_{ij}^{-1}. \tag{9}$$

Therefore, the response of the detector is given by the number of photons per energy bin as

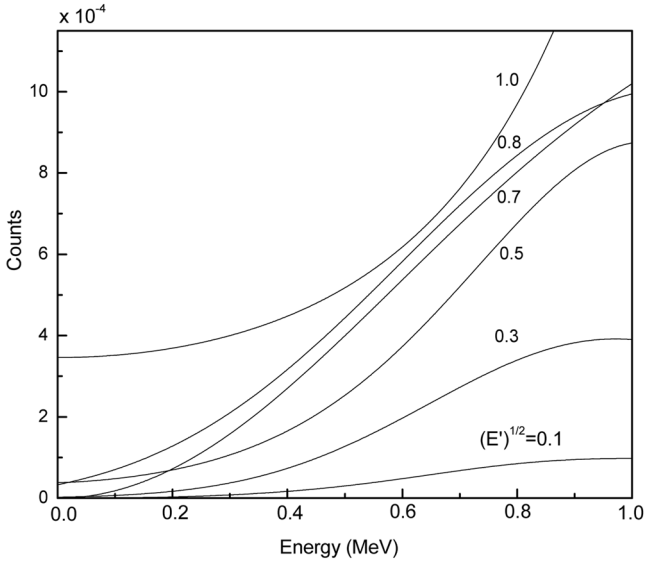

FIG. 8. Interpolated bin content counts vs incident energy at different values of $(E')^{1/2}$.

TABLE I. Response matrix **R** with elements R_{ij}, of the NaI(Tl) detector. The $E^{1/2}$ values refer to tops of energy bins. Each row corresponds to a pulse-height distribution due to a line source of energy $E-\Delta E/2$ normalized to the efficiency of the crystal. 10^{-3} should multiply the numbers.

$(E')^{1/2}$ / $(E)^{1/2}$	0.1	0.2	0.3	0.4	0.5	0.6	0.7	0.8	0.9	1.0
0.1	999									
0.2	2	998								
0.3	2	17	981							
0.4	3	20	27	949						
0.5	4	18	22	40	894					
0.6	5	18	25	42	69	742				
0.7	6	16	25	39	54	71	610			
0.8	6	15	25	37	49	63	72	487		
0.9	6	15	25	37	49	57	62	66	385	
1.0	5	14	22	33	46	49	53	54	55	327

$$N(E) = \frac{N_i}{E_i - E_{i-1}}, \tag{10}$$

where $N(E)$ is in units of photons per unit energy interval and is the response-corrected spectrum. Figure 9 shows a typical continuous pulse-height distribution and resultant spectrum for radiations from ^{203}Hg (E_x=74 keV and E_γ =279 keV). Low pulse-height counts resulting from partial absorption of higher energy photons are shifted to the photopeak energy. The events left in the Compton continuum in the lower bin meshes account for partial and/or complete absorption of 74 keV x rays, back scattered events, and the events resulting from a lower portion of a full energy peak lying in the bin adjacent to peak the energy bin mesh.

V. RESULTS AND DISCUSSIONS

A typical observed spectrum [curve (a)] from the copper target (thickness 10 mm) at a scattering angle of 60°, exposed to 662 keV γ photons is given in Fig. 10. The observed pulse-height distributions are a composite of singly as well as multiply scattered photons along with background events. Curve (b) of the Fig. 10 gives observed background spectrum with the copper target out of the primary beam and thus corresponds to events unrelated to the target. Subtraction of events under curve (b) from those under curve (a) results in a scattered spectrum [curve (c) of Fig. 10] corresponding to events originating from the interaction of 0.662 MeV primary γ photons with the target material and subsequent events such as multiple Compton scattering, bremsstrahlung, Rayleigh scattering, etc. The observed spectrum consists of intensity distribution of singly as well as multiplies scattered photons. The singly scattered events under the full energy peak are obtained by reconstructing analytically (details given in Sec. II) the singly scattered inelastic peak using the experimental determined parameters, such as FWHM and the detector efficiency of the detector corresponding to the singly scattered energy, counts at the photo

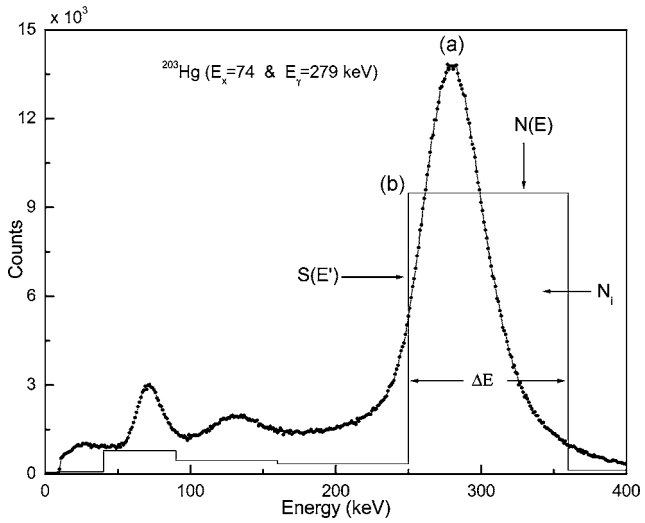

FIG. 9. A typically experimentally observed pulse-height distribution $S(E')$, (curve *a*) and a resulting calculated histogram (curve *b*) of $N(E)$ with ^{203}Hg source.

TABLE II. Inverted response matrix $\mathbf{R}_{ij}^{-1}$, in the same units as Table I. 10^{-3} should multiply the numbers.

$(E')^{1/2}$ / $(E)^{1/2}$	0.1	0.2	0.3	0.4	0.5	0.6	0.7	0.8	0.9	1.0
0.1	1000									
0.2	−2	1002								
0.3	−2	−17	1019							
0.4	−3	−21	−29	1054						
0.5	−4	−19	−24	−47	1119					
0.6	−6	−21	−30	−55	−104	1348				
0.7	−8	−20	−34	−57	−87	−157	1639			
0.8	−9	−21	−39	−60	−86	−151	−242	2053		
0.9	−11	−24	−44	−68	−98	−148	−222	−352	2597	
1.0	−9	−23	−38	−61	−97	−127	−188	−280	−437	3058

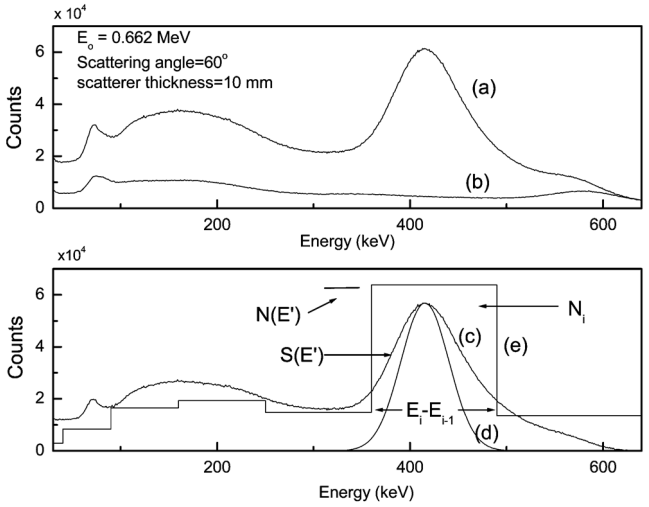

FIG. 10. A typical experimentally observed spectrum [curve (a)] of 0.662 MeV incident photons with 10 mm thick copper target at a scattering angle of 60° for 10 ks irradiation time. Observed background spectrum for 10 ks without a copper target in the primary beam [curve (b)]. Experimentally observed pulse-height distribution, $S(E')$, [curve (c)] obtained after subtracting background events. Normalized analytically reconstructed singly scattered full energy peak [curve (d)] and resulting calculated histogram [curve (e)] of $N(E)$ converting pulse-height distribution to a photon spectrum.

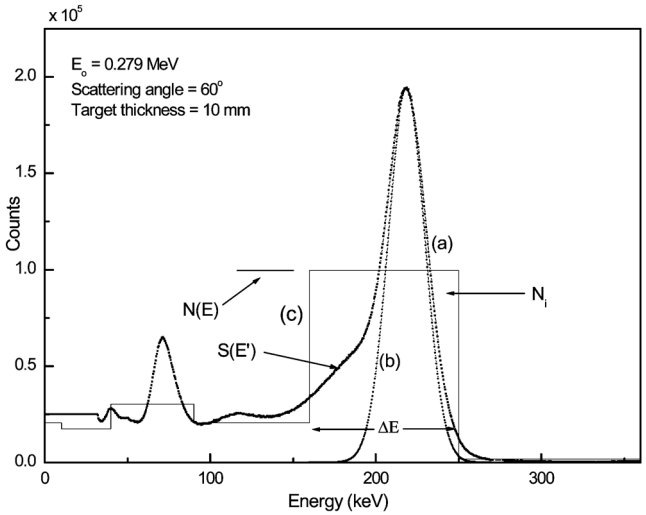

FIG. 11. Curves having a similar description as in Fig. 10 for 0.279 incident photons.

peak, and Gaussian distribution of inelastically scattered peak. The analytically reconstructed singly scattered peak is shown by curve (d) of Fig. 10.

The experimental pulse-height distribution [curve (c)] is converted to a photon energy spectrum with the help of an inverse response matrix (given in Sec. IV). Curve (c) of Fig. 10 provides experimental pulse-height distribution $S(E')$ for radiation originating from interactions of 0.662 MeV incident γ photons with the electrons of 10 mm thick copper target with γ detector placed at 60° to incident beam. The solid curve (e) is the resulting calculated histogram of $N(E)$ in units of photons. Low pulse-height counts resulting from a partial absorption of higher energy photons are shifted to the photopeak energy. The events under the histogram in the Compton continuum accounts for photons of reduced energy (less than that of inelastically Compton scattered peak) originating from multiple interactions in the target and finally escaping in the direction of γ detector. The events under the calculated histogram corresponding to energy range from 360 to 490 keV accounts for singly and multiply scattered radiations having energy equal to that of singly scattered ones. The events under curve (d) of Fig. 10 are divided by peak-to-total ratio, $\varepsilon_p(E)$, of the γ detector and then their subtraction from the events under the calculated histogram [curve (e)] in the specified energy range results in events not originating from singly Compton scattering but having the same energy as in singly Compton scattering. These residual events are divided by intrinsic (crystal) efficiency and when corrected for the iodine escape peak [16,17] and absorption in the aluminum window [18] of the detector, provides the emergent flux from the copper scatterer at 60° having energy in the range of inelastically scattered peak distribution. The intensity of photons, corresponding to respective selected bin meshes in which the singly scattered Compton peak distribution lies, emerging from copper targets when these are exposed to 0.279 MeV γ photons (Fig. 11) from a ^{203}Hg source and 1.12 MeV γ photons (Fig. 12) from a ^{65}Zn source is also calculated in a similar manner.

The plot of a observed number of multiply scattered events, corresponding to respective different bin meshes for the three different incident photon energies, as a function of target thickness, is shown in Fig. 13. The solid curves provide the best-fitted curves corresponding to the present experimental data. The present experimental results show that the number of multiply scattered events, for each of the incident photon energy, increases with an increase in the target thickness and saturates after a particular value of target thickness, called saturation depth. The saturation of multiply scattered photons is due to the fact that as the thickness of

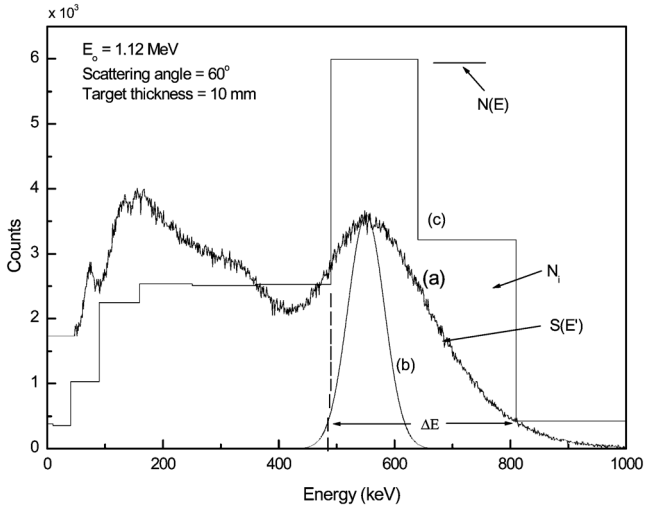

FIG. 12. Curves having a similar description as in Fig. 10 for 1.12 MeV incident photons.

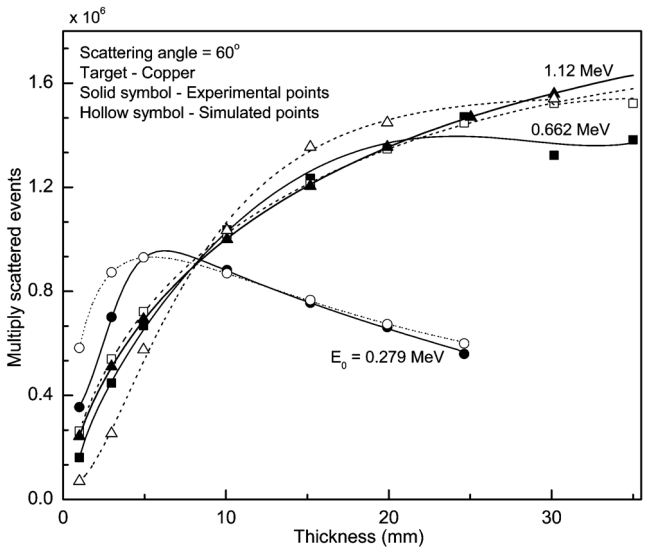

FIG. 13. Variation of an observed number of multiply scattered events as a function of thickness of the copper target for different incident photon energies.

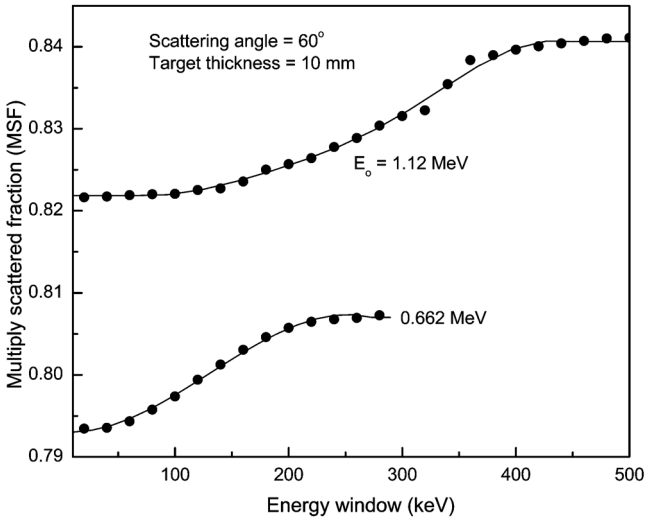

FIG. 14. Plot of multiply scattered fractions (MSF) as a function of energy windows around the Compton scattered peak centroid for 0.662 and 1.12 MeV incident photon energies,

the target increases, the number of scattered events also increases but the number of photons coming out of the target decreases. So a stage is reached when the thickness of the target becomes sufficient to compensate the above increase and decrease of the number of photons. The thickness for which the number of multiply scattered photons saturates in copper target is 5, 20, and 23 mm for 0.279, 0.662, and 1.12 MeV incident photons, respectively. The mean free path in copper is 9.46, 15.37, and 20.07 mm for the respective incident photon energies. The saturation thickness increases with an increase in incident photon energy and is less than two mean free paths. A small decrease in the intensity of multiply scattered photons at a further increasing target thickness is due to absorption and further attenuation of scattered radiation in the target before reaching the detector.

The present experiment is simulated with the Monte Carlo package developed by Bauer and Pattison [19]. The Monte Carlo package has been tested for a different number of photons entering the sample and it has been found that there is no appreciably change in the fractional intensity of multiply scattered distribution. The results based upon Monte Carlo calculations for multiply scattered intensity, at a scattering angle of 60° for three different incident photon energies in our geometrical conditions, are also given in Fig. 13. The dotted curves are the best-fitted curves corresponding to the simulated data. The simulated data of multiply scattered intensity increase with an increase in target thickness and then saturates for the three different incident photon energies. The saturation value is found to be increasing with increase in incident photon energy. This behavior of simulated data supports the present experimental results. It is important to mention here that the Monte Carlo package used by us is applicable to stationary electrons only.

As the thickness of the target increases the wings of the Compton scattered peak are broadened due to multiple scattering which concentrates approximately at the lower half of the scattered peak. The top half of the peak has a negligible amount of multiple scattering and is determined by a factor called the MSF. This factor contributes a background signal which reduces the quality of the image in Compton scatter imaging for a nondestructive testing of samples [9], and is expressed as

$$(\mathrm{MSF}) = \frac{M_{\mathrm{m}}}{M_{\mathrm{m}} + M_{\mathrm{s}}}, \tag{11}$$

where M_{m} and M_{s} are the numbers of multiply and singly scattered photons under the Compton scattered peak. In the present study, a copper target of a very small thickness of 1 mm considered to have a negligible amount (4.5% of saturation value) of multiple scattering (at 0.662 MeV incident energy) is chosen for the determination of M_{s}. The area under the Compton scattered peak with this target is subtracted from the area under the experimentally measured Compton scattered peak with thick targets to obtain the amount of multiply scattered photons only. For this purpose, the exact position of the centroid of the scattered peak is required and is calculated with the help of Compton's formula [Eq. (2)] for a given energy. An energy window of about 20 keV is chosen across this centroid and the area under this energy window is determined. Next, the width of the energy window is increased by 20 keV, and the area under the peak is noted. This procedure, of increasing the window width by 20 keV, is repeated and the MSF value for each window is determined. Figure 14 shows that the MSF starts saturating above an energy window of about 200 and 400 keV for 0.662 and 1.12 MeV incient energies, respectively, which means that multiple scattering is concentrated in the lower part of the Compton scattered peak in the energy range from 360 to 490 keV (for 0.662 MeV incident photons), that is near the valley of the peak. On the other hand, as the energy window is decreased, the MSF decreases to a very low value depicting that, at the Compton scattered peak, the multiple scattering contribution is negligibly small (less than 5%). A

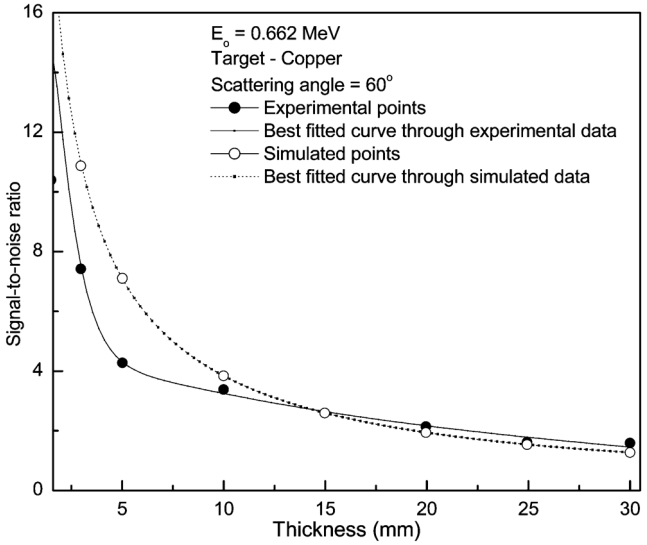

FIG. 15. Variation of signal-to-noise ratio as a function of target thickness for 0.662 MeV photons.

similar behavior of saturation of MSF value at the energy window of 180 keV is observed for 0.279 MeV incident photons.

In Compton profiles [1] and cross-section measurements, only the singly scattered photons entering the detector are desired and the multiply scattered photons act as background noise. The signal-to-noise ratio (ratio of the number of singly scattered events to number of multiply-scattered events) is plotted as a function of target thickness for 0.662 MeV incident photons (Fig. 15). It is clear that when the target thickness increases, the signal-to-noise ratio decreases, indicating the presence of more multiply scattered events in comparison to the singly scattered events. The Monte Carlo calculations also support this behavior. A similar behavior is observed for 0.279 and 1.12 MeV incident photons. In order to increase the signal-to-noise ratio, multiple scattering backgrounds should be minimized which can be achieved using thin targets.

Our present results confirm that for thick targets, there is significant contribution of multiply scattered radiation emerging from the scatterer, having energy equal to that of singly scattered Compton process. The present measurements of multiple scattering of 0.279 and 1.12 MeV incident photons are observed by us for the first time. The saturation of intensity of multiple scattering events beyond a particular thickness supports the work of Paramesh *et al.* [6]. The saturation thickness increases with an increase in incident photon energy. Monte Carlo calculations of multiply scattered intensity and signal-to-noise ratio support the present experimental data. The saturation of MSF above a particular energy window around the centroid of an inelastic scattered peak supports the work of Barnea *et al.* [9]. The signal-to-noise ratio decreases with an increase in target thickness. The detector response unfolding converting the observed pulse-height distributions to a photon energy spectrum is quite satisfactory. The work on multiple scattering is further in progress for targets of different atomic numbers and under different geometrical conditions. The simulated and experimental data show similar behavior. The deviation of some of the simulated points from the experimental values may be caused by noninclusion of multiply scattered contribution from the moving electrons, which is not available in the present package. It is further planned to modify the present Monte Carlo package to include the effect of moving electrons on multiply scattered intensity for better understanding of the multiple scattering processes.

[1] M. J. Cooper, Rep. Prog. Phys. **48**, 415 (1985).
[2] Manpreet Singh, Gurvinderjit Singh, B. S. Sandhu, and Bhajan Singh, Appl. Radiat. Isot. **64**, 373 (2006).
[3] B. G. Williams and V. Halonen, Phys. Fenn. **10**, 5 (1975).
[4] V. Halonen, B. G. Williams, and T. Paakkari, Phys. Fenn. **10**, 107 (1975).
[5] V. Halonen and B. Williams, Phys. Rev. B **19**, 1990 (1979).
[6] L. Paramesh, L. Venkataramaiah, K. Gopala, and H. Sanjeevaih, Nucl. Instrum. Methods Phys. Res. **206**, 327 (1983).
[7] T. Pitkanen, D. Laundy, R. S. Holt., and M. J. Cooper, Nucl. Instrum. Methods Phys. Res. A **251**, 536 (1986).
[8] T. Pitkanen, M. J. Cooper, D. Laundy, and R. S. Holt, Nucl. Instrum. Methods Phys. Res. A **257**, 384 (1987).
[9] G. Barnea, C. E. Dick, A. Ginzburg, E. Navon, and S. M. Seltzer, NDT & E Int. **28**, 155 (1995).
[10] N. Shengli, Z. Jun, and H. Liuxing, Proceedings of the Second International Workshop on EGS (KEK Proceedings 200-20, Tsukuba, Japan, 2000), pp. 216–223.
[11] V. Halonen, I. R. Epstein, A. C. Tanner, and B. G. Williams, *Multiple Scattering. In Compton Scattering* (McGraw-Hill, Book, New York, 1977), pp. 79–101.
[12] J. H. Hubbell, Rev. Sci. Instrum. **29**, 65 (1958).
[13] J. H. Hubbell and N. E. Scofield, IRE Trans. Nucl. Sci. **NS-5**, 156 (1958).
[14] C. E. Crouthamel, *Applied Gamma-ray Spectrometry* (Pergamon Press, London, 1960), pp. 202–216, 673.
[15] S. D. Conte and C. Boor, *Elementary Numerical Analysis* (Tata McGraw-Hill, New Delhi, 1980), p. 160.
[16] P. Axel, Rev. Sci. Instrum. **25**, 39 (1954).
[17] W. J. Veigele, At. Data **5**(1), 51 (1973).
[18] J. H. Hubbell, Radiat. Res. **70**, 58 (1977).
[19] Gerrit E. W. Bauer and P. Pattison, *Compton Scattering Experiments at the HMI* (Hahn-Meitner-Institute Für Kernforschung, Berlin, 1981) HMI-B 364, pp. 1–106.